International Journal of Fracture **122:** 47–64, 2003.
© 2003 *Kluwer Academic Publishers. Printed in the Netherlands.*

Thermo-Mechanical Failure Criterion at the Micron Scale in Electronic Devices

Z. YOSIBASH[1], O. ADAN[2], R. SCHNECK[2] and H. ATLAS[3]
[1]*Dept. of Mechanical Engineering, Ben-Gurion University of the Negev, Beer-Sheva, Israel (e-mail address: zohary@bgumail.bgu.ac.il)*
[2]*Dept. of Material Engineering, Ben-Gurion University of the Negev, Beer-Sheva, Israel*
[3]*Tower Semiconductors, POBox 619, Migdal Haemek, Israel*

Submitted 20 May 2002; revised version 1 March 2003

Abstract. Thermo-mechanical failures may occur in the passivation layer of micro-electronic devices during the fabrication process. These are in form of cracks which initiate at keyhole corners. In order to predict and eventually prevent these cracks a failure criterion is presented, based on an average value of the elastic strain energy in the vicinity of a reentrant corner of any angle. The proposed strain energy density (*SED*) failure criterion is validated by a test including 24 full size wafers which have been fabricated with different parameters: the interconnects (metal lines) height, the passivation thickness, and the passivating plasma power which was shown to correlate with the mechanical properties of the passivation layer. For each wafer, a FE model has been constructed, and the *SED* computed. It has been clearly shown, that above the critical value of $SED_{cr}[R = 0.15\mu m] \approx 1000\ [J/m^3]$, all wafers manufactured were cracked. The *SED* criterion seems to correlate well with the empirical observations, and may be used as a standard tool for the mechanical design of failure free micro-electronic devices.

1. Introduction

The fabrication of micro-electronic devices (chips) is a multi-step process aimed at creating a layered structure made of semiconductors, metals and insulators. Thin aluminum interconnect lines are fabricated by sputtering technology on top of which the passivation is deposited by PECVD (Plasma Enhanced Chemical Vapor Deposition). At this last step of the fabrication process, the wafer is heated to approximately 400 °C, and the passivation Si_3N_4 layer is deposited to cover the metalic lines. Then, the wafer is cooled to room temperature, at which stage mechanical failures in the form of cracks are sometimes encountered. A typical layered structure before and after the passivation layer is deposited is shown in Figure 1. The cracks are often detected on 'test chips' placed on the silicon wafer (typically of diameter of 6, 8 or 12 inches (0.1524, 0.2032 or 0.3048 m)) among the many chips fabricated on same wafer. The 'test chips' are manufactured so to represent the worst possible configurations which increase their affinity to failure. I.e. if failure does not initiate in them (mechanical, functional, etc.), all other chips on the wafer are fail safe (see Figure 2). Previous work indicated that these cracks, emanating in the passivation layer at reentrant corners are due to the thermal loading caused when cooling the wafer in the last step of fabrication. Thermal stresses in confined metal lines during thermal cycling have been experimentally investigated by Moske et al. (1993), where it was demonstrated that these can lead to damage formation in the passivation. The cause for the cracks is identified as a mismatch of the elastic constants and thermal expansion coefficients between the metal lines and the passivation layer. Typical cracks can be observed

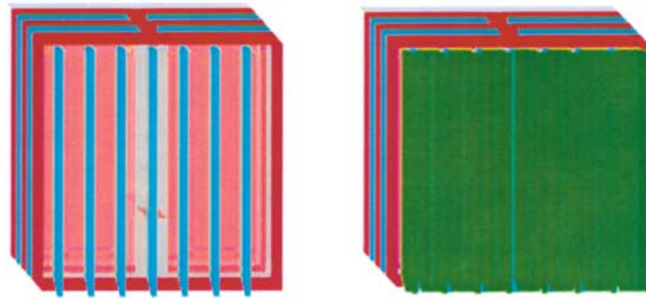

Figure 1. The layered structure of a typical chip. The first offwhite layer is the silicon substrate, the red layers are insulators, the blue layers as well as the thin blue lines are made of metals, and the passivation layer is green.

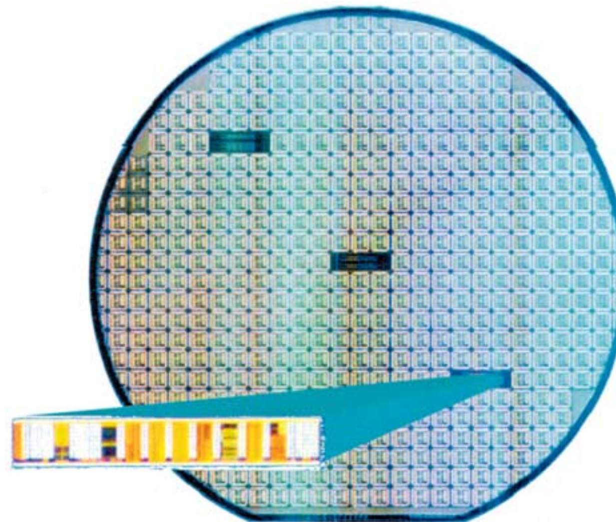

Figure 2. The silicon wafer patterned with hundreds of square dies. The unpatterned areas are the scribes. The 3 wide rectangles dies are the test chip arrays seen in the blowup.

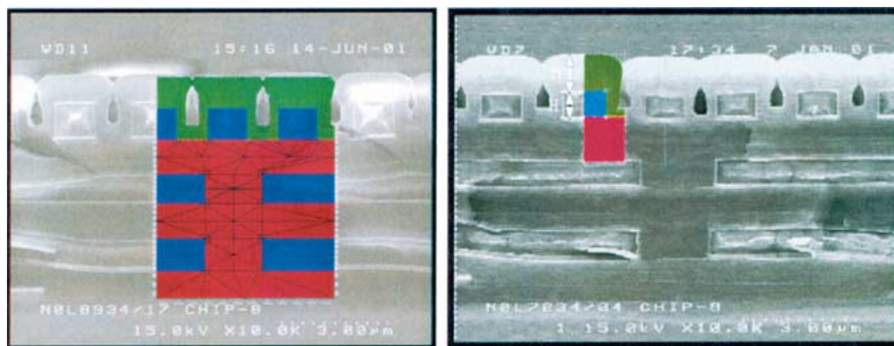

Figure 6. Finite element models superimposed in color on the SEM cross section of the test chip device. Blue-Aluminum, Red-SiO_2 dielectric and Green-Si_3N_4 passivation.

by sectioning the wafer at the test chip followed by a scanning electron microscope (SEM) inspection, as shown in Figure 3.

Zoom-in figures of a typical top view and cross section of failed components show that the failure initiates at the vertex of a reentrant V-notch (keyhole corner) – as shown in Figure 4.

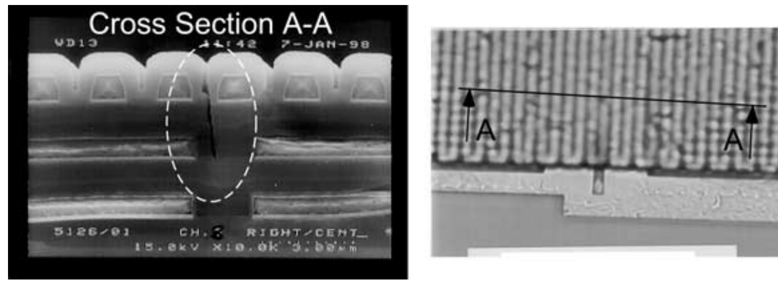

Figure 3. Cracks in the passivation layer: on the right a top view of the wafer, on the left a Scanning Electron Microscope image of the cross-section.

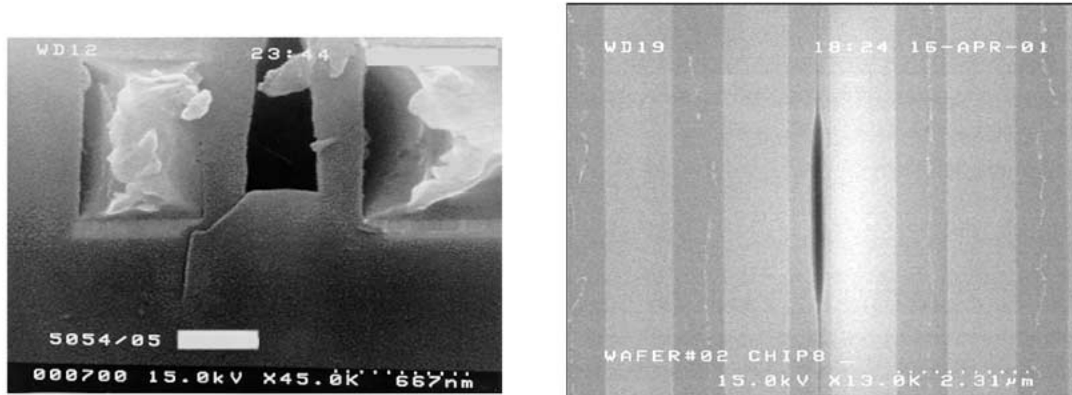

Figure 4. Top view of a crack (right) and a zoom-in at a cross-section (left) of typical failure initiation sites in the passivation layer (SEM image).

In an attempt to predict and eventually prevent these failures, a combined analytical-numerical and experimental research has been conducted, which is presented herein. The typical feature dimension of the studied electronic devices are 0.1 to 1 μm where the assumptions of linear elasticity still hold, see e.g. Brandt et al. (1992). In this case, the V-notch tip, where failure initiates, is a singular line at which the elastic stress tensor tends to infinity. Because failures are manifested by long planar cracks along reentrant V-notch tip lines in the passivation, a plane strain analysis of a cross-section represents well the problem. Same assumptions have been adopted in previous theoretical investigations of stress singularities by Michael and Hartranft (1991) and Miyoshi et al. (1992). They used finite element analysis (FEA) for the computation of the singular stress field in the vicinity of singular points under thermal loading, and concluded their work by suggesting of further research for formulating a failure criterion. Sauter and Nix (1990) used FEA to investigate the thermal stresses in passivated lines bonded to substrates. Their work indicates that thermal stresses depend on the line width (increasing dramatically with decreasing its aspect ratio), the passivation material and geometry (increasing with thicker and stiffer passivation).

Wan et. al (1999) investigated failure initiation at a 90 degrees re-entrant corner in a micromechanical silicon structure. They correlated the critical mode I stress intensity to fracture initiation, using it as the failure initiation criterion. This approach is well suited for a constant V-notch angle, but is not suited for V-notches of varying opening angles. Mazza and Dual (1999) proposed a failure criterion for a silicon micromechanical structure having a re-entrant corner of 135 degrees. It is based on the equilibrium of the strain energy in a radial sector of

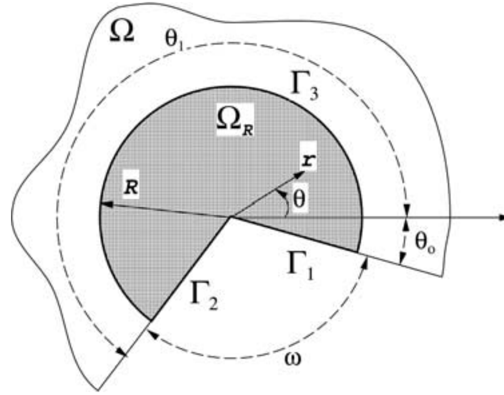

Figure 5. The domain of interest and notations.

radius R and thickness h and the surface energy required to create a crack of same length R along a thickness h, in a specific direction in silicon. Since the strain energy increases non-linearly as a function of the radial sector R, while the surface energy increases linearly in R, there exists a radius R_{cr} (equals to 0.8 nm for silicon) where the strain energy distribution equals the surface energy for crack creation. This critical radius (which of course is material dependent) is chosen in their paper as the failure criterion. Mazza and Dual's criterion applies well to plane stress situations (very thin structural layers) and requires the knowledge of the specific surface energy of the materials of interest. Since we are interested in a different geometry (plane strain situation), and the specific surface energy is not known, a different approach is advocated.

This paper is organized as follows: we first introduce and formulate a mechanical failure criterion in passivation layers, denoted by strain energy density (*SED*). In section 3 we identify the fabrication parameters which have the largest influence on the failure initiation. As shall be shown, the mechanical properties and shape of the passivation layer and the metal lines have a dominant influence on the failure. Therefore, the material properties of the various layers have to be measured. In section 4 the failure criterion (*SED*) is validated via an experimental program. It involves the fabrication of wafers with different values of critical parameters, followed by a numerical procedure for the computation of the *SED* associated with each of the fabricated wafers. To establish the critical value $(SED)_{cr}$ under which no failures are observed, the experimentation had been carried out in three phases. In section 5 we summarize the obtained $(SED)_{cr}$, and demonstrate that under a threshold value no failures are observed, validating the proposed failure criterion.

2. The Strain Energy Density Failure Criterion

It is conceivable to assume that failure initiates when the average elastic strain energy contained in a sector around the singular point, over the volume of this sector, reaches a critical value. This averaged elastic strain energy density we denote by strain energy density (*SED*).

Consider a circular sector Ω_R of radius R centered in the singular point (this is the V-notch tip at which the failure initiates):

$$\Omega_R \stackrel{\text{def}}{=} \{(r, \theta) \mid 0 \le r \le R,\ \theta_0 \le \theta \le \theta_1\},$$

with traction free boundary conditions on the faces intersecting at the singular point (Figure 5). Assume that a constant temperature change of $\Delta\tau = constant$ is imposed, so that the uncoupled isotropic thermo-elastic problem to be solved, under the assumption of **plane-strain** is given by:

$$\mu\nabla^2\mathbf{u} + (\lambda+\mu)grad\ div\ \mathbf{u} = \mathbf{0} \quad in\ \Omega_R \tag{1}$$

$$\left(2\mu\varepsilon_{ij}(\mathbf{u}) + \lambda\varepsilon_{kk}(\mathbf{u})\delta_{ij}\right)\mathbf{n} = \alpha(3\lambda+2\mu)\Delta\tau\mathbf{n} \quad on\ \theta = \theta_0, \theta_1 \tag{2}$$

summation notation is implied unless otherwise specified, λ and μ are the Lamé material constants, and $\mathbf{u} = (u_1, u_2)^T$ denotes the displacements in x_1 and x_2 directions. The strain tensor is computed from the displacements using the standard kinematic connections:

$$\varepsilon_{ij} = \tfrac{1}{2}(\partial_i u_j + \partial_j u_i)$$

The displacements in the vicinity of the singular point, namely the solution of the thermo-elastic system, consist of two parts. A homogeneous part $\mathbf{u}^H$, as if no thermal loading is present in the *neighborhood of the singularity*, Ω_R, and a particular part $\mathbf{u}^{Th}$, which is the particular solution chosen so to satisfy the non-homogeneous right-hand-side of the thermo-elastic system in Ω_R. The homogeneous solution can be represented as (see e.g. [9]):

$$\mathbf{u}^H = \sum_{i=1}^{\infty} A_i r^{\alpha_i} \begin{Bmatrix} u_1^{(i)}(\theta) \\ u_2^{(i)}(\theta) \end{Bmatrix} \Longrightarrow \boldsymbol{\sigma}^H = \sum_{i=1}^{\infty} A_i r^{\alpha_i - 1} \begin{Bmatrix} \sigma_{11}^{(i)}(\theta) \\ \sigma_{22}^{(i)}(\theta) \\ \sigma_{12}^{(i)}(\theta) \end{Bmatrix} \tag{3}$$

where α_i are the singularity exponents, with $\alpha_1 \le \alpha_2 \le \alpha_3 \cdots$ (for cracks $\alpha_1 = \alpha_2 = 1/2$), and A_i's depend on the thermal loading away from the singular point, and directions 1 and 2 mean x_1 and x_2. The particular solution due to a constant temperature increase is given by (see [10, p. 11], [11]):

$$\mathbf{u}^{Th} = \beta\Delta\tau \begin{Bmatrix} x_1 \\ x_2 \end{Bmatrix} \tag{4}$$

where $\beta = \frac{\alpha(3\lambda+2\mu)}{2(\lambda+\mu)}$.

It is easily seen that:

$$\varepsilon_{ij} = \varepsilon_{ij}^H + \varepsilon_{ij}^{Th}, \qquad with \quad \varepsilon_{ij}^{Th} = \beta\Delta\tau\delta_{ij}, \quad i, j = 1, 2. \tag{5}$$

The connection between the stress tensor and *elastic* strain tensor is given for an isotropic elastic material via the Hooke's law. The 'homogeneous' part of the strain tensor $\boldsymbol{\varepsilon}^H$ is the so-called 'elastic' part of the total strain. For *plane strain* conditions the stress tensor is:

$$\sigma_{ij} = 2\mu\varepsilon_{ij}^H + \lambda\varepsilon_{kk}^H\delta_{ij}. \tag{6}$$

For plane strain:

$$\varepsilon_{33} = 0 = \varepsilon_{33}^H + \alpha\Delta\tau \tag{7}$$

thus $\varepsilon_{33}^H = -\alpha\Delta\tau$, and

$$\begin{aligned} \sigma_{33} &= \lambda\varepsilon_{ii} - \alpha(3\lambda+2\mu)\Delta\tau \\ &= \lambda\varepsilon_{ii}^H - 2\lambda\beta\Delta\tau - \alpha(\lambda+2\mu)\Delta\tau \\ &= \lambda\varepsilon_{ii}^H - \alpha\frac{\mu(3\lambda+2\mu)}{\lambda+\mu}\Delta\tau \end{aligned} \tag{8}$$

We now proceed and define the elastic strain energy $\mathcal{U}(\mathbf{u})[R]$. For a fully 3-D domain:

$$\mathcal{U}(\mathbf{u})[R] \stackrel{\text{def}}{=} \frac{1}{2} \iiint_{\Omega_R \times b} \sigma_{mn} \varepsilon_{mn}^H d\Omega, \qquad m, n = 1, 2, 3 \tag{9}$$

For a domain of constant thickness b, the elastic strain energy can be split into two:

$$\begin{aligned} \mathcal{U}(\mathbf{u})[R] &= \frac{1}{2} b \iint_{\Omega_R} \left[2\mu \varepsilon_{ij}^H \varepsilon_{ij}^H + \lambda \left(\varepsilon_{kk}^H \right)^2 \right] d\Omega + \frac{1}{2} b \iint_{\Omega_R} \sigma_{33} \varepsilon_{33}^H d\Omega \\ &\stackrel{\text{def}}{=} \mathcal{U}^H[R] + \mathcal{U}^*[R] \end{aligned} \tag{10}$$

the first term is associated with the stresses and strains acting in-plane, and the second term reflects the stresses and strains perpendicular to it.

We first concentrate our attention to $\mathcal{U}^H[R]$. Using Green's theorem, the area integral is first transformed into a boundary integral, which is zero along Γ_1 and Γ_2, thus

$$\begin{aligned} \mathcal{U}^H[R] &= \frac{1}{2} b \int_{\partial \Omega_R} \left(2\mu \varepsilon_{ij}^H + \lambda \varepsilon_{kk}^H \delta_{ij} \right) n_j u_i^H dS \\ &= \frac{1}{2} b \int_{\theta_0}^{\theta_1} \left[\left(2\mu \varepsilon_{ij}^H + \lambda \varepsilon_{kk}^H \delta_{ij} \right) n_j u_i^H \right]_{r=R} R \, d\theta \end{aligned} \tag{11}$$

inserting (3) in the above:

$$\begin{aligned} \mathcal{U}^H[R] = \tfrac{1}{2} b \textstyle\sum_{k,\ell} A_k A_\ell R^{\alpha_k + \alpha_\ell} \int_{\theta_0}^{\theta_1} \Big[& \sigma_{11}^{(k)}(\theta) u_1^{(\ell)}(\theta) \cos\theta + \sigma_{12}^{(k)}(\theta) \\ & \left(u_1^{(\ell)}(\theta) \sin\theta + u_2^{(\ell)}(\theta) \cos\theta \right) + \sigma_{22}^{(k)}(\theta) u_2^{(\ell)}(\theta) \sin\theta \Big] d\theta \end{aligned} \tag{12}$$

For isotropic materials, with traction free boundary conditions in the neighborhood of the singular point, the following orthogonality relation holds (see Yosibash and Szabó, 1995):

$$\int_{\theta_0}^{\theta_1} \left[\sigma_{11}^{(k)} u_1^{(\ell)} \cos\theta + \sigma_{12}^{(k)} \left(u_1^{(\ell)} \sin\theta + u_2^{(\ell)} \cos\theta \right) + \sigma_{22}^{(k)} u_2^{(\ell)} \sin\theta \right] d\theta = 0 \quad for \quad k \neq \ell \tag{13}$$

which simplifies (12) to:

$$\begin{aligned} \mathcal{U}^H[R] = \tfrac{1}{2} b \textstyle\sum_k A_k^2 R^{2\alpha_k} \int_{\theta_0}^{\theta_1} \Big[& \sigma_{11}^{(k)} u_1^{(k)} \cos\theta + \sigma_{12}^{(k)} \left(u_1^{(k)} \sin\theta + u_2^{(k)} \cos\theta \right) \\ & + \sigma_{22}^{(k)} u_2^{(k)} \sin\theta \Big] d\theta \end{aligned} \tag{14}$$

Now, consider $\mathcal{U}^*[R]$, after substituting of equation (8)

$$\begin{aligned} \mathcal{U}^*[R] &= \frac{1}{2} b \iint_{\Omega_R} \left(\lambda \varepsilon_{ii}^H - \alpha \frac{\mu(3\lambda + 2\mu)}{\lambda + \mu} \Delta\tau \right) \varepsilon_{33}^H d\Omega \\ &= -\frac{1}{2} b \alpha \Delta\tau \left[\lambda \iint_{\Omega_R} \varepsilon_{ii}^H d\Omega + \alpha \frac{\mu(3\lambda + 2\mu)}{\lambda + \mu} \Delta\tau \Omega_R \right] \end{aligned} \tag{15}$$

It is important to note that $\mathcal{U}^*[R]$ is the strain energy generated due to a strain component in the x_3 direction, hence is not of importance for a crack initiation in the $x_1 - x_2$ plane and

will not be taken into consideration. Thus we define the *in-plane* strain energy density (*SED*) as:

$$SED[R] \stackrel{\text{def}}{=} \frac{\mathcal{U}^H[R]}{b \times \Omega_R}$$

and using (14), we finally obtain:

$$\begin{aligned} SED[R] = \textstyle\sum_k A_k^2 \frac{R^{2\alpha_k - 2}}{(\pi - \frac{\omega}{2})} \int_{\theta_0}^{\theta_1} \Big[\sigma_{11}^{(k)} u_1^{(k)} \cos\theta + \sigma_{12}^{(k)} \left(u_1^{(k)} \sin\theta + u_2^{(k)} \cos\theta \right) \\ + \sigma_{22}^{(k)} u_2^{(k)} \sin\theta \Big] d\theta \end{aligned} \tag{16}$$

For the problems treated herein, where a constant temperature change is imposed ($\Delta\tau =$ *const*), the second thermal generalized stress intensity factor is zero, $A_2 \equiv 0$. Thus, (16) can be written as:

$$SED[R] = A_1^2 \frac{R^{2\alpha_1 - 2}}{(\pi - \frac{\omega}{2})} I_1 + A_3^2 \frac{R^{2\alpha_3 - 2}}{(\pi - \frac{\omega}{2})} I_3 + \mathcal{O}(R^{2\alpha_4 - 2}) \tag{17}$$

where

$$I_k \stackrel{\text{def}}{=} \int_{\theta_0}^{\theta_1} \Big[\sigma_{11}^{(k)} u_1^{(k)} \cos\theta + \sigma_{12}^{(k)} \left(u_1^{(k)} \sin\theta + u_2^{(k)} \cos\theta \right) + \sigma_{22}^{(k)} u_2^{(k)} \sin\theta \Big] d\theta$$

is the integral of the k-th eigen-pair. To demonstrate that the second and further terms in (17) are negligible in comparison with the first term, consider the ratio of the second term over the first term, denoted by γ:

$$\gamma = \left(\frac{A_3}{A_1} \right)^2 R^{2(\alpha_3 - \alpha_1)} \frac{I_3}{I_1} \tag{18}$$

For problems at which the opening angle is $0 \le \omega \le \pi/2$, $\alpha_1 \approx 0.5$ and $\alpha_3 \approx 1$ to 1.5, so that $2(\alpha_3 - \alpha_1)$ is between 1 to 2. The ratio $\frac{I_3}{I_1}$ is close to 1 because the eigen-pairs are normalized so that the normalization factor is reflected in the coefficients A_i's. The values of A_3 in all our numerical investigations are at the same order of magnitude as A_1, and in most cases are smaller, so that $\frac{A_3}{A_1} = \mathcal{O}(1)$. Thus one obtains:

$$R^2 \lesssim \gamma \lesssim R^1 \tag{19}$$

If $R << 1$ (we used in our computation $R = 0.15\mu m$), the terms in the series (16) for which $\alpha_k > 1$ are orders of magnitude smaller compared to the first term, thus negligible, simplifying (16) to:

$$\begin{aligned} SED[R] \approx \frac{A_1^2}{R^{2(1-\alpha_1)}(\pi - \frac{\omega}{2})} \int_{\theta_0}^{\theta_1} \Big[\sigma_{11}^{(1)} u_1^{(1)} \cos\theta + \sigma_{12}^{(1)} \left(u_1^{(1)} \sin\theta + u_2^{(1)} \cos\theta \right) \\ + \sigma_{22}^{(1)} u_2^{(1)} \sin\theta \Big] d\theta \end{aligned} \tag{20}$$

To numerically test that (20) approximates well the strain energy density, we computed the *SED*$[R]$ using the stresses and strains according to (9), and compared to these obtained by using (20). For all cases they match within less than 3% difference. The *SED*$[R]$ depends of course on a characteristic length size R. It should be chosen small enough so that Ω_R is within the K-dominance region, ensuring that the singular terms do represent the exact solution. The

small difference between the $SED[R]$ first computed by (20), and the ones computed by (9) ensures that the chosen radius R is not too large. Given the value of $SED[R_1]$, one can easily determine the value of *SED* for a domain having a different radius R_2 by the simple equation derived from (20):

$$SED[R_2] = SED[R_1]\left(\frac{R_1}{R_2}\right)^{2-2\alpha_1} \tag{21}$$

A characteristic material dependent R can be determined for macroscopic domains, which is a function of the ultimate stress and the critical stress intensity factor, but for microscopic domains considered in this paper, these parameters are unavailable. We chose R as a characteristic dimension of 0.15μm and report all results for this value.

The SED proposed above reminds the well known SED criterion by Sih and Macdonald (1974), however it is considerably different in several respects. The SED of Sih is a *pointwise value* evaluated at any point on an arc located at a radius R away from the crack tip and is usually applied to crack tip singularities. Because it is a function of θ, a minimum value can be found at a given angle θ^*. Thus, Sih's SED may be used as a criterion for predicting the crack propagation direction. Correlated to a critical material dependent parameter, it can be used also as a failure criterion. The SED failure criterion proposed herein is an *avaraged value*, is not aimed at predicting directions of crack propagation, but at predicting failure initiation at a specific critical value for any opening angle of the V-notch.

3. Material Properties

The electronic device in the neighborhood of the failures (Figure 6) is a layered structure made of the passivation layer (Si_3N_4 green colour in the Figure), the metal lines under the passivation and in the dielectric (made of aluminum, blue colour in the Figure) and the SiO_2 dielectric shown in red. It has been observed that failures if occur, initiate at one of the reentrant corners above the gap in the wide metal lines. Simulating of a small portion as shown in the right part of Figure 6 does not mimic important details and there is a need to simulate a larger portion as shown in the left part of Figure 6. There are several parameters which may contribute to the failure initiation, however, the design rules allow to change three during the fabrication process, namely:

(a) the thickness of the passivation layer (denoted by h),

(b) the height of the metal lines (denoted by H),

(c) plasma power applied during the chemical vapor deposition of the passivation layer.

Passivation thickness has two effects. First, the deposition PECVD process has a relatively poor step coverage, and therefore tends to form overhangs resulting in 'keyholes' (e.g. Sze, 1983, p. 95) and singular points. Second, the reentrant angle tends to zero as the passivation thickness increases until a given thickness, and the strength of the singularity is more severe (see Figure 7), then, beyond $h \approx 6500\text{Å}$, the angle slightly increases again.

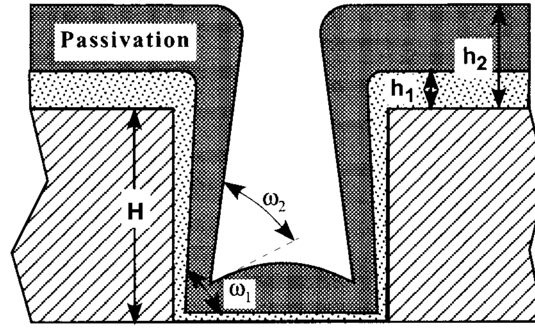

Figure 7. Nonconformal step coverage of deposited passivation film

3.1. Material properties of passivation layers.

Variation of the plasma power causes different chemical reactions (silane and ammonia) during the chemical vapor deposition of the silicon nitride. This in turn causes variation in the thermal expansion coefficient α and the Young modulus E (Poisson ratio ν is assumed to remain constant). Hence a correlation between material properties and the plasma power was necessary. These can be evaluated from measurements of residual stresses incurred in a bi-material domain under thermal loading. A useful method to evaluate these stresses in thin films is the Stoney method described in Tu et al. (1992, pp. 409–413). Unpatterned layers of Si_3N_4 were deposited with different plasma powers and different thicknesses on circular Si wafers at the ordinary elevated temperature, and then cooled to room temperature. The residual stress in each wafer was determined from the curvature of the bi-material wafer.

Properties of thin layers of Si_3N_4 found in the literature indicate a large variation (see e.g. Tu et al. (1992)). Starting with typical values of E, and α, we varied them in order to match the measured residual stresses in the wafers. A unique evaluation of the material properties could have been obtained by using two different substrate materials, however, this was not available for this research. It was found that with increasing power, E increases and α decreases, obeying the equations:

$$E(W) = 0.682 \exp(0.0097 \times W) \quad [\text{GPa}] \tag{22}$$

$$\alpha(W) = 1.22 \times 10^{-4} \exp(-0.0224 \times W) \quad [1/C^o] \tag{23}$$

(where W stands for the plasma power in Watts). Figure 8 summarizes the results, the exponential fit equations and the table lists the material properties.

Equations (22–23) are used for evaluating the material properties associated with each plasma power.

Because the material properties E and α are temperature dependent, the above fit represents their averaged value between the deposition temperature (400 °C) and room temperature.

A simplified finite element model as shown in the right side of Figure 6 was used to investigate the influence of several other fabrication parameters on the strength of the singularity. It was found that the height of the metal lines H has a large influence while the width seemed to have little to no influence. Therefore H was chosen as the third parameter of investigation. The simplified finite element model has also been used to verify that the 'plastic radius' (the maximal length measured from the V-notch tip where the equivalent stress is above yielding) is negligible compared to the passivation thickness.

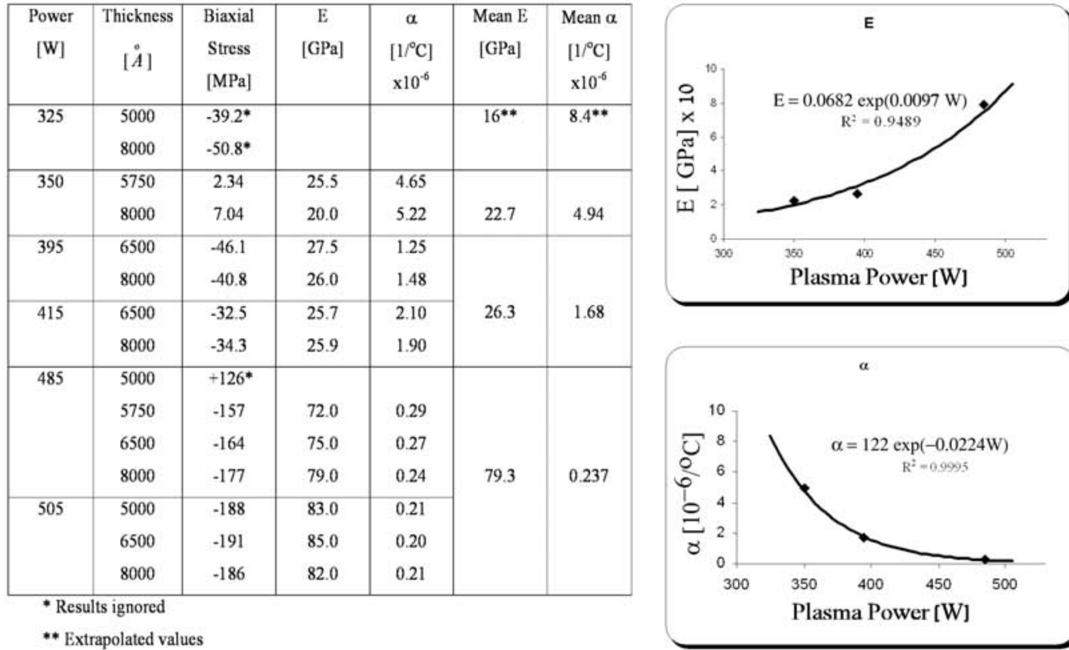

Power [W]	Thickness [Å]	Biaxial Stress [MPa]	E [GPa]	α [1/°C] x10^{-6}	Mean E [GPa]	Mean α [1/°C] x10^{-6}
325	5000	-39.2*			16**	8.4**
	8000	-50.8*				
350	5750	2.34	25.5	4.65		
	8000	7.04	20.0	5.22	22.7	4.94
395	6500	-46.1	27.5	1.25		
	8000	-40.8	26.0	1.48		
415	6500	-32.5	25.7	2.10	26.3	1.68
	8000	-34.3	25.9	1.90		
485	5000	+126*				
	5750	-157	72.0	0.29		
	6500	-164	75.0	0.27		
	8000	-177	79.0	0.24	79.3	0.237
505	5000	-188	83.0	0.21		
	6500	-191	85.0	0.20		
	8000	-186	82.0	0.21		

* Results ignored

** Extrapolated values

Figure 8. Passivation material properties vis. plasma power

Table 1. Material properties (E, ν and α) - A survey

Property	Al line interconnect	SiO_2 diel.	Si_3N_4 pass.	Ref.
E [GPa]	71.5	71.7	150	[5]
	63.9*	72.9*	30	[16]
	35 nm / 100 nm / bulk	–	–	
	24.1 / 16.5 / 62	–	–	[15]
ν	0.35	0.16	0.25	[5]
	0.36*	0.17*	0.22	[16]
α ($10^{-6}/C^o$)	23.6*	0.55*	1	[5]
	$23.434 + 6.996\Delta\tau/10^3 + 248.1(\Delta\tau)^2/10^6$	–	1.1	[14]

*Value used in our computations.

3.2. Aluminum lines and dielectric layers

For the proposed failure criterion, the Young modulus (E), Poisson ratio (ν), and the coefficient of thermal expansion (α) of the aluminum lines and SiO_2 dielectric layers are also essential. These are known to vary according to the nature of their deposition and their minor scale lengths. A literature survey shows different values for the aluminum lines. Experiments by Steinwall and Johnson (1990) on aluminum fibers removed from substrates to produce free standing fibers of 8mm long 1μm (grain sizes of 35 and 100 nanometers) show Young modulus of the range of 16–24 GPa. However, Ohring (1992, p. 426) and Tu et al. (1992) lists Young modulus of evaporated thin films similar to these of bulk. In our numerical simulations we used the material properties marked by * in Table 1: for the SiO_2 dielectric the material

Table 2. Fabrication parameters and results of phase 1 of the experiments

Wafer #	H [Å]	h [Å]	Plasma Power [Watt]	Cracked?
1	7000	5000	305	Cracked
2	7000	8000	305	Cracked
3	7000	5000	485	Cracked
4	7000	8000	485	Not Cracked
5	11000	5000	305	Cracked
6	11000	8000	305	Cracked
7	11000	5000	305	Cracked
8	11000	8000	305	Not Cracked
9	9000	6500	305	Cracked

properties do not vary in different references, so that $E = 72.9$ GPa, $\nu = 0.17$ and $\alpha = 10^{-6}$ $1/C^o$. For the Aluminum lines we used the the values $E = 68.9$ GPa, $\nu = 0.36$ and $\alpha = 23.6$ $1/C^o$. For the Si_3N_4 passivation we used E and α from (22), and $\nu = 0.22$.

4. Experimental validation of the failure criterion

Validation of the failure criterion requires the same critical value of the *SED* to be obtained for different configurations of the device. A set of experiments have been designed to test the hypothesis, and herby to determine the failure envelope. Past experience showed that the failure envelope resides within the following extreme limits:

1. Al lines of height $7000\ \mathring{A} \le H \le 11000\ \mathring{A}$ with the standard being $H = 9000\ \mathring{A}$.
2. Si_3N_4 thickness of $5000\mathring{A} \le h \le 8000\mathring{A}$ with the standard being $h = 6500 \pm 300\ \mathring{A}$.
3. Plasma power of $305\ Watts \le p \le 485\ Watts$ with the standard being $395 Watts$ (E and α for Si_3N_4 computed by (22)).

Phase 1 of the experiments consisted of nine wafers fabricated as full factorial design of experiment (3 parameters, 2 levels + 1 center point). The precise manufacturing parameters of the nine wafers is listed in Table 2, and their visualization, in a form of a 'test-cube' is shown in Figure 9. The last column of Table 2 indicates whether a crack was detected in the passivation layer after fabrication.

Based on the results of phase 1, at high plasma power and thick passivation , failure does not occur, regardless of the metal thickness.

For refining the failure envelope another fifteen wafers were fabricated in phases 2 and 3, with parameters which lie between any pair of cracked and intact wafers from phase 1. Table 3 summarizes phases 2 and 3 fabrication parameters. All the 24 wafers were examined for cracks in a SEM by cross sectioning, and selected pictures for 6 of the wafers are shown in Figure 10. In order to correlate the experimental observations with the proposed failure criterion, one needs to compute the *SED* associated with each tested wafer. This procedure is described in the following subsection.

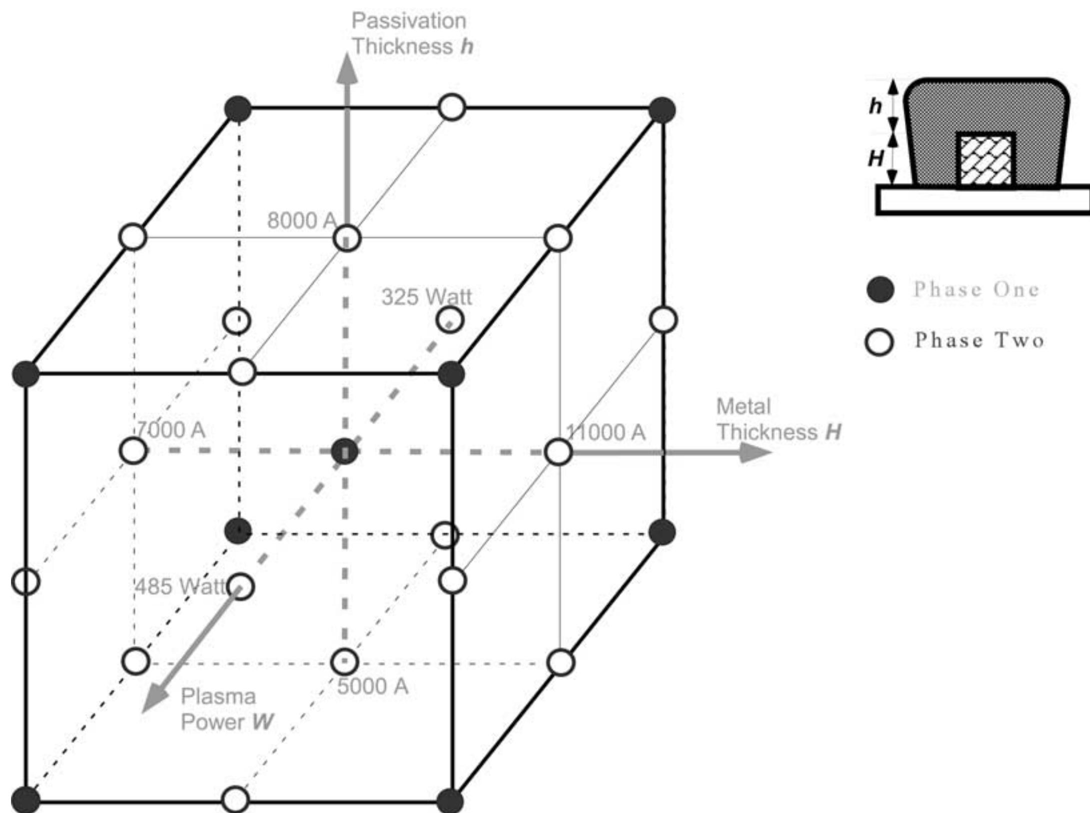

Figure 9. The 'test-cube' illustrating the different fabrication parameters in the test plan. The full circles represent phase one experiment where the center is the standard parameters.

Table 3. Fabrication parameters of phase 2&3 tests

Wafer #	H [Å]	h [Å]	Plasma Power [Watt]	Cracked?
10	7000	6500	415	Not Cracked
11	7000	6500	515	Not Cracked
12	7000	8000	415	Not Cracked
13	11000	5750	485	Cracked
14	11000	8000	350	Cracked
15	11000	5750	350	Cracked
16	7000	6500	515	Not Cracked
17	7000	8000	415	Not Cracked
18	7000	6500	415	Not Cracked
19	9000	8000	515	Not Cracked
20	9000	8000	395	Crack roots
21	9000	6500	515	Not Cracked
22–24	9000	6500	395	Cracked

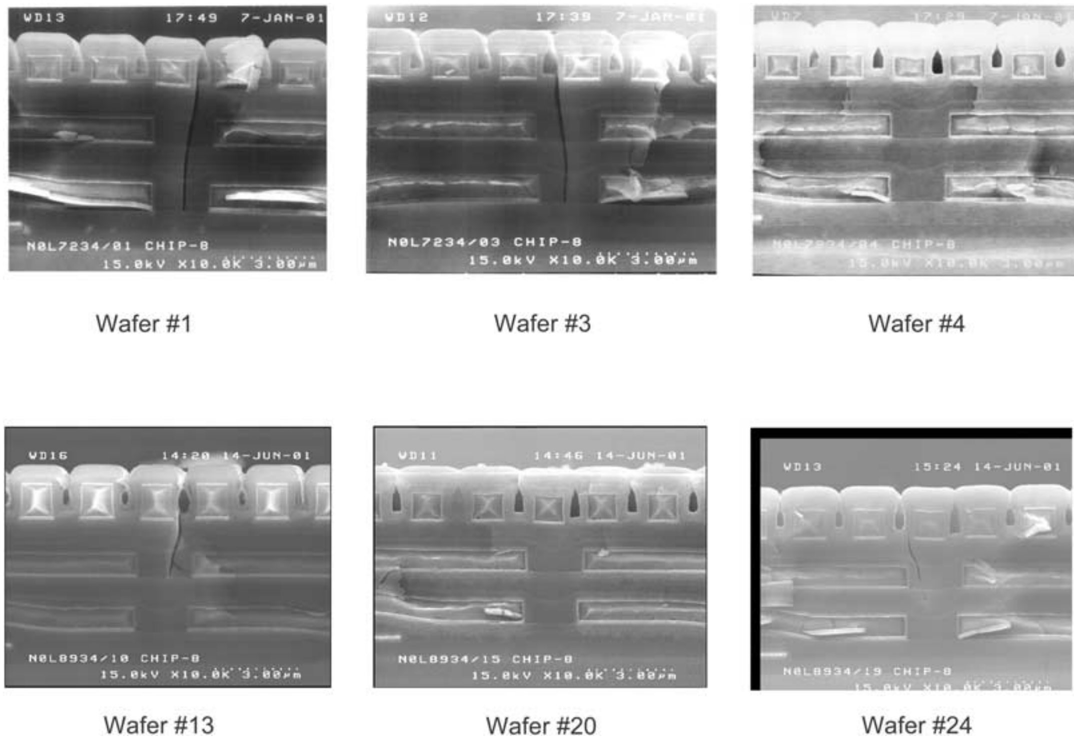

Figure 10. Selected SEM cross sections from the 24 tested wafers.

4.1. Computing *SED*s by p-version FEM.

The precise dimensions and the geometry in the neighborhood of the singular points has been measured for each of the tested wafers, and a p-version parametric finite element model has been constructed, as shown in the left picture of Figure 6. By varying these parameters, each of the 24 tested wafers have been represented. These models consist up to two main designs:

1. Models with passivation thickness of up to 5750 Å.
2. Models with passivation thickness between 6500 Å and 8000 Å.

The reason for the two different models is because, as was seen in the SEM cross-sections, the passivation tends to connect and close up on top of the keyholes, leaving the keyholes open. Another important difference is contributed to the non-conformal step coverage. The passivation is thicker on horizontal walls, and thinner on the vertical walls. During the initial stages of the passivation process (around 5000 Å), a ‘hill’ is built in the middle of the keyhole, having sharp angles therefore increasing the stress singularity. Continuation of the deposition and the closing of the rooftop around h =5750 to 6500 Å, causes the sharp ‘crack-like’ tips to become no longer sharp. Figure 11 presents the finite element models used for phase 1 wafers. The p-FEM commercial code StressCheck[1] has been used in our computations. The polynomial degree has been increased over each element from 1 to 8, using the product space. This code has been chosen for the following reasons:

[1]StressCheck is trademark of Engineering Software Research and Development, Inc, St. Louis, MO, USA

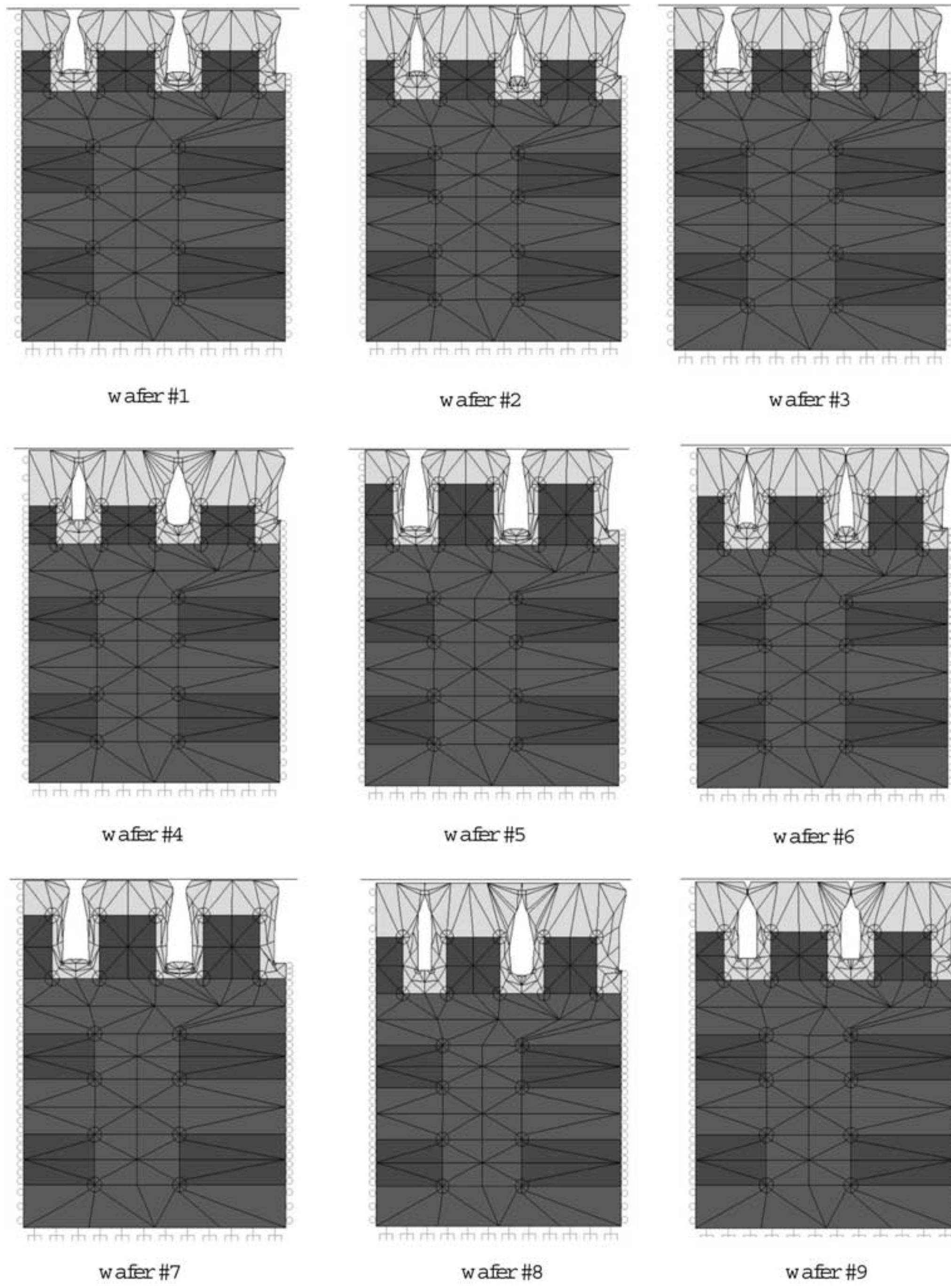

Figure 11. Finite element models simulating phase 1 wafers.

Table 4. SED for tested wafers.

Wafer #	H [Å]	h [Å]	Plasma Power [Watts]	E [GPa]	α [$1/C^o$]	ν	$SED^*[R = 0.15\mu m]$ [J/m^3]
1	7000	5000	325	16.0	8.40E–06	0.22	**114,000**
2	7000	8000	325	16.0	8.40E–06	0.22	**124,000**
3	7000	5000	485	79.3	2.37E–07	0.22	**1,380**
4	7000	8000	505	82.0	2.10E–07	0.22	985
5	9000	6500	395	25.7	1.25E–06	0.22	**4,430**
6	11000	5000	325	16.0	8.40E–06	0.22	**108,000**
7	11000	8000	325	16.0	8.40E–06	0.22	**121,000**
8	11000	5000	485	79.3	2.37E–07	0.22	**1,350**
9	11000	8000	505	82.0	2.10E–07	0.22	88.8
10	7000	6500	415	25.7	2.1E–06	0.22	664
11	7000	6500	515	85.0	2E–07	0.22	25.5
12	7000	8000	415	25.9	1.9E–06	0.22	985
13	11000	5750	485	79.3	2.37E–07	0.22	**1,260**
14	11000	8000	350	22.7	4.94E–06	0.22	**54,400**
15	11000	5750	350	22.7	4.94E–06	0.22	**52,400**
16	7000	6500	515	79.3	2.4E–07	0.22	25.5
17	7000	8000	415	26.3	1.7E–06	0.22	985
18	7000	6500	415	26.3	1.7E–06	0.22	664
19	9000	8000	515	79.3	2.37E–07	0.22	13.6
20	9000	8000	395	26.3	1.68E–06	0.22	612
21	9000	6500	515	79.3	2.37E–07	0.22	39.2
22	9000	6500	395	26.3	1.68E–06	0.22	**4,430**
23	9000	6500	395	26.3	1.68E–06	0.22	**4,430**
24	9000	6500	395	26.3	1.68E–06	0.22	**4,430**

*Bold face numbers indicate failures.

- The numerical error is reported and can thus be controlled. In our computations all models are under 1% error in the energy norm (see e.g. [17]).
- Curved boundaries are represented accurately, and large aspect ratios of the elements do not deteriorate the accuracy of the results.
- Special optimal mesh design using geometric progression of the elements with a factor of 0.17 towards singular points ensures high accuracy and exponential convergence rates.
- The eigen-pairs $(\alpha_i, \mathbf{u}^{(i)}(\theta))$ of (3) are being computed and reported for any singular point (see details in [12]).
- The thermal generalized stress intensity factors A_i's are computed accurately and reported together with the eigen-pairs (see [11]).

Using the eigen-pairs, the A_i and an integration radius of $R = 0.15\mu m$, the SED in the vicinity of the singular points has been computed for all test wafers, and summarized in Table 4. To visualize the failure envelope, all wafers are shown on the test-cube together with the *SED* values in Figure 12.

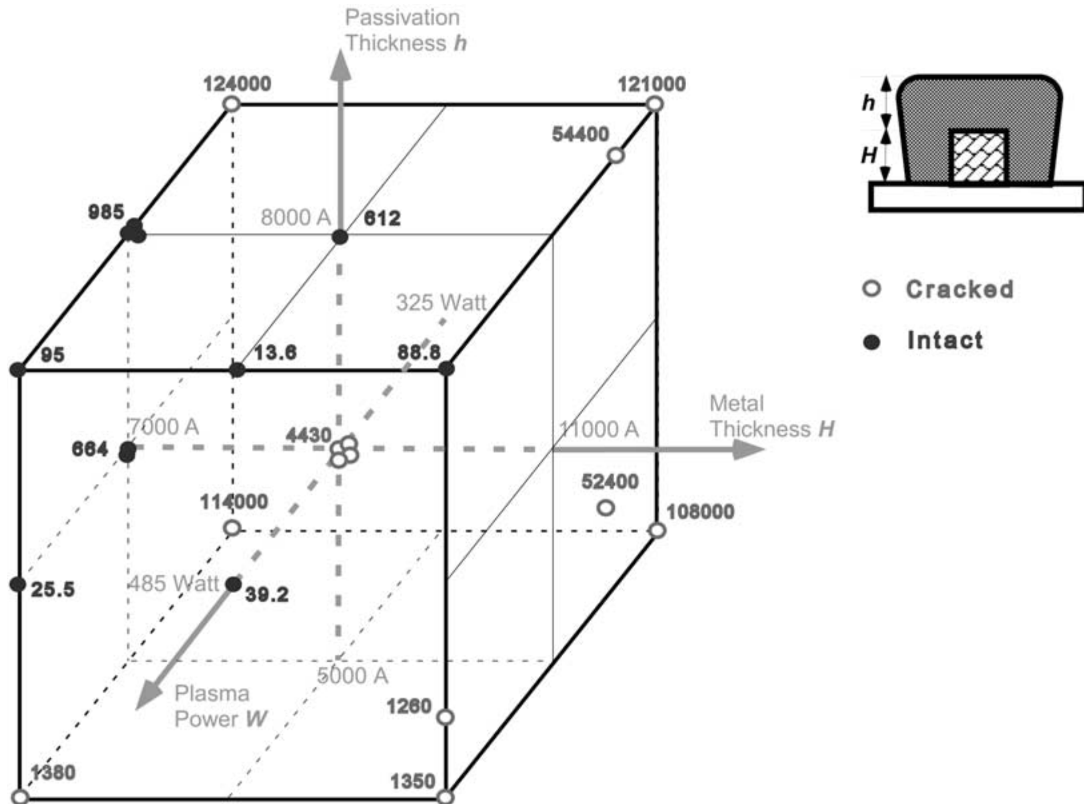

Figure 12. Mapping of SEDs on the 'test-cube' (Units are J/m^3). The variation of the SED appears to reflect the mechanical status of the devices.

A semi-cylindrical failure envelope is observed, assessing the proposed criterion. A single value of the *SED* distinguishes between the cracked and intact wafers - under a threshold value of $SED_{cr}[R = 0.15\mu m] \approx 1000$ $[J/m^3]$, all wafers manufactured are intact.

5. Summary and Conclusions

In the fabrication process of electronic devices, cracks may emanate at the vertex of key-holes reentrant corners in the passivation layers. These failures are believed to be due to thermal loading at the final cooling stage of the electronic device. To enable the prediction and eventually preventing of such failures a failure criterion has been presented, formulated and experimentally validated. It is based on the elastic strain energy density absorbed in the vicinity of a reentrant corner of any angle. Because of the very small dimensions of the site where failures occur, we estimated the zone where plastic deformation occur in the vicinity of the reentrant corner, to verify that the elastic assumption is valid. Computations fully support the assumption because the plastic zone is orders of magnitude smaller than the scale length of the Al lines or passivation thickness.

To validate the SED criterion's applicability to the electronic industry, a test plan has been designed so to obtain the SED_{cr} below which failures are not observed. Because failure initiation depends on several physical parameters, we limited this research to three of them which can be easily changed in the fabrication process: the Al lines height, the passivation

thickness, and the plasma power which was shown to correlate with the mechanical properties of the passivation layer. Fabricating 24 wafers with different values of these parameters, we succeeded to obtain wafers free of failures as well as cracked wafers. For each wafer, a FE model has been constructed, and the *SED* computed. It has been clearly shown, that above the critical value of $SED_{cr}[R = 0.15\mu m] \approx 1000\ [J/m^3]$, all wafers manufactured were cracked, for the three tested parameters. The proposed *SED* criterion seems to correlate well with the empirical observations, and may be used as a standard tool for the mechanical design of failure free electronic devices. This has major advantages because it shortens time to market by using simulation tools in place of trial and error fabrication processes.

Acknowledgement

The support of this work by the Israel Ministry of Industry and Commerce under 0.25μ Consortium Grant is gratefully acknowledged.

The authors gratefully acknowledge the anonymous referees for their valuable and constructive comments and for bringing to our attention other papers related to the topic of the present one, leading to improvements in the presentation and context.

References

Moske, M.A., Ho, P.S. , Mikalsen, D.J., Cuomo, J.J. and Rosenberg, R. (1993), Measurement of thermal stress and stress relaxation in confined metal lines. 1. stress during thermal cycling. *Jour. App. Phys.*, **74(3)**: 1716–1724.

Brandt, O., Ploog, K., Bierwolf R. and Hohenstein, M. (1992), Breakdown of continuum elasticity theory in the limit of monoatomic films. *Physical Review Letters*, **68(9)**: 1339–1342.

Michael, M.M. and Hartranft, R.J. (1991), Thermal stress singularities in microelectronic. In *Proceedings - 41st Electronic Components & Technology Conference, Atlanta, GA, USA*, pages 273–277. IEEE, Piscataway, NJ.

Miyoshi, T. , Shiratori, M., Okuda, H. and Takano, N. (1992), Stress singularities at the interface crack and the corner of edge-bonded dissimilar materials. *Advances in Electronic Packaging - ASME*, pages 551–557.

Sauter, Anne I. and Nix, W.D. (1990), Finite element calculations of thermal stresses in passivated and unpassivated lines bonded to substrates. In *Materials Research Society Symposium Proceedings*, volume 188, pages 15–21.

Wan, S.W. , Dunn, M.L. , Cunningham, S.J. and Read, D.T. (1999), Elastic moduli, strength, and fracture initiation at sharp notches in etched single crystal silicon microstructures. *Jour. Appl. Phy.*, **85(7)**: 3519–3534.

Mazza, E. and Dual, J. (1999), Mechanical behavior of a μm-sized single crystal silicon structure with sharp notches. *Jour. Mech. Phy. Sol.*, **47**: 1795–1821.

Sih, G.C. and Macdonald, B. (1974), Fracture mechanics applied to engineering problems - strain energy density fracture criterion. *Eng. Fracture Mechanics*, **6**: 361–386.

Kondratiev, V.A. (1967), Boundary value problems for elliptic equations in domains with conical or angular points. *Transact. Moscow Math. Soc.*, **16**: 227–313.

Rössle, A. (1996), Spannungssingluraritaten fur gekoppelte strukturen in der festkorpermechanik unter mechanisher und thermischer belastung. Master's thesis, Universitat Stuttgart, Mathematishes Institut A, Stuttgart, Germany, January.

Yosibash, Z. (1998), Thermal generalized stress intensity factors in 2-d domains. *Computer Meth. Appl. Mech. Engrg.*, **157**: 365–385.

Yosibash, Z. and Szabó, B.A. (1995), Numerical analysis of singularities in two-dimensions. Part 1: Computation of eigenpairs. *Int. Jour. Numer. Meth. Engrg.*, **38**(12):2055–2082.

Sze, S.M. (1983), *VLSI Technology*. McGraw-Hill.

Tu, King-Ning, Mayer, James W. and Feldman, Leonard C. (1992), *Electronic Thin Film Science for Electrical Engineers and Material Scientists*. Macmillan Publishing Company.

Steinwall, James E. and Johnson, H.H. (1990), Mechanical properties of thin film aluminum fibers: Grain size effects. In M.F. Doerner, W.C. Oliver, G.M. Pharr, and F.R. Brotzen, editors, *Materials Research Society Symposium Proceedings – 188*, pages 177–183. MRS.

Ohring, Milton. (1992), *The Materials Science of Thin Films*. Academic Press.
Szabó, B.A. and Babuška, I. (1991), *Finite Element Analysis*. John Wiley & Sons, New York.